Turk J Phys
26 (2002) , 199 – 207.

Structural Analysis of a GaAs/Al_xGa_{1-x} As Hot Electron Light Emitter Using Double Axis X-Ray Diffraction

Ali TEKE
Balıkesir University, Faculty of Art & Science, Department of Physics,
10100 Balıkesir-TURKEY
e-mail : ateke@balikesir.edu.tr

Received 01.05.2001

Abstract

We report on interference peaks in double axis x-ray rocking curves of tunable wavelength hot electron light emitters. The device is based on a p-GaAs and n-$Ga_{1-x}Al_xAs$ heterojunction containing an inversion layer on the p- side, and GaAs quantum wells on the n- side of the junction, a construction known as HELLISH-2 (Hot Electron Light Emitting and Lasing in Semiconductor Heterostructure-Type 2). The interference has been shown to strongly depend on the periodicy of the device structure. Experimental curves are compared with simulated rocking curves. Some structural parameters, such as total epilayer thickness, composition ratio and quantum well width and barrier width were obtained. It has been shown that double axis x-ray diffraction is a very helpful for the device designer as well as the crystal grower.

Key Words: X-ray diffraction, structural analysis, semiconductor devices, hot electrons, LED

1. Introduction

III-V compound quantum wells, superlattices and thin epitaxial layers are of great interest due to their optical and electronic properties. To understand these properties fully, it is extremely important to know accurately the structural parameters, such as epilayer thickness, period of superlattice, lattice strain (mismatch) with respect to the substrate and chemical composition.

Double axis x-ray diffraction is an essential and widely used technique to investigate these structural parameters due to its unique properties, such as high sensitivity to any strain, precision and non-destructive characteristics. X. Chu and B. K. Tanner [1]observed interference peaks in double crystal x-ray rocking curves for the $Al_xGa_{1-x}As$ laser structure, which arise from the phase coherence of the x-ray waves across the thin heteroepitaxial layer sandwiched between two layers of equal composition. Structural investigations of several different epitaxial systems, such as AlSb/GaSb superlattice grown on GaSb [2], Si/Si_xGe_{1-x}heterostructure [3], $Ga_xIn_{1-x}As_{1-y}P_y$ systems grown on InP substrate [4] and InGaAs/InP grown on InP substrate [5]as well as GaAs/$Al_xGa_{1-x}As$ heterostructure quantum well systems [6, 7, 8] were also reported during the last decade by using this technique.

In this work, we have considered three HELLISH-2 samples coded as ES1, ES2 and ES6. Structural parameters of these samples were obtained by using double axis x-ray diffraction. Experimental and simulation results are compared with the growth parameters. They are used as real growth parameters in our theoretical modelling of HELLISH-2 structures, which is used to optimise device operation. Electrical and optical properties of these devices, together with their possible optoelectronic applications, have been reported elsewhere [9, 10, 11, 12]. Theoretical modelling has also been studied in these papers.

2. Sample Structures and Growth Parameters

The samples ES2, ES1 and ES6 were grown by Molecular Beam Epitaxy (MBE) in a Varian Modular III system. Figure 1(a) shows the schematic representation of the structure of ES2 and ES1. They were grown on Cr-doped semi-insulating GaAs substrates oriented in the $< 100 >$ direction. The substrate temperature was kept constant at 580°C during the growth of all epilayers. For ES2 the layer sequence starts with the growth of 4 μm thick undoped GaAs buffer layer on top of the SI substrate. For sample ES1 the GaAs buffer layer is intentionally p-doped by Be with doping density of about $N_A \sim 5\text{x}10^{16}$ cm^{-3}. For both samples, the rest of the structure is identical. The buffer layer is followed by ten periods of a five-layer compound substructure. At the center of each substructure is a 75 Å GaAs quantum well. Both above and below this are 110 Å of undoped $Al_xGa_{1-x}As$ (x=0.33) as spacers. Sandwiching these three layers are layers of 75 Å thick Si-doped $Al_xGa_{1-x}As$ (x=0.33) with $N_D \sim 8\text{x}10^{17}$. Following the ten periods of multiple quantum wells is a 225 Å thick Si-doped $Al_{0.33}Ga_{0.67}As$ ($N_D \sim 8\text{x}10^{17}$ cm^{-3}), then capped with a 240 Å thick undoped GaAs layer to prevent oxidation of the $Al_{0.33}Ga_{0.67}As$ layer below.

Figure 1(b) shows the schematic structure of ES6. The main difference between this sample and ES2 and ES1 is the inclusion of two quantum wells with smaller well widths, $L_z = 50$Å on top of 75Å wells at the junction plane. For ES6, all the epitaxial layers were deposited on a $< 100 >$ oriented Cr-doped semi-insulating substrate. The growth was initiated by growing a 4 μm thick (Be) p-type doped GaAs buffer layer on top of the substrate with a doping density of $N_A \sim 5\text{x}10^{16}$ cm^{-3}. The buffer layer is followed by four periods of a five-layer compound structure (denoted by the letter "A" in Fig. 1(b)), then 110 Å of undoped $Al_xGa_{1-x}As$ (x=0.33) as spacer, then by two periods of another five layer compound structure (denoted by the letter "B" in Fig. 1(b)). Substructures A are identical to the five-layer substructures in Fig. 1(a). Substructure B are identical to A except at the center is a 50 Å GaAs quantum well. Above substructures B is, as in Fig. 1(a), a 225 Å layer of Si-doped $Al_{0.33}Ga_{0.67}As$ ($N_D \sim 8\text{x}10^{17}$ cm^{-3}). The growth was completed by capping with 240 Å undoped GaAs layer to prevent oxidation the of $Al_{0.33}Ga_{0.67}As$ layer below.

3. Experimental Techniques

The investigation was carried out by using a high-resolution computer-controlled double crystal x-ray diffractometry in a nondispersive (+n, -m) setting at 004 surface symmetric reflection. A highly perfect Si [111] crystal was used as a reference crystal. The Si reference crystal and GaAs specimen were used at the same time but were displaced from parallel position in order to get simultaneous diffraction. A Water-cooled Enraf-Nonius 3502 model 35V and 35 mA x-ray generator with a copper target to produce $CuK_{\alpha 1}$(λ=0.1540562 nm) radiation as x-ray source coupled to a Bede Model 200 diffractometer with an angular resolution of 0.5 arcsecond was used in the experiment. This diffractometer is capable of rocking curve analysis on III-V compound structures. Figure 2 shows the schematic diagram of the experimental setup.

The principle on which double axis x-ray diffractometers work is the comparison of the lattice parameter of the specimen with that of a reference crystal. To do this, x-rays coming from the target is conditioned in wavelength in a (+n,-n,+n,-n) setting sequence by means of Channel-Cut Collimator (CCC) which consists of a silicon crystal in the channel oriented for the symmetric reflection. The conditioned beam is then diffracted at the Bragg angle by the reference crystal. The reference crystal is used as a true monochromator. The diffracted beam emerging from the reference crystal is incident onto the specimen crystal, but is also oriented at the Bragg angle. The diffracted beam from the specimen is detected by a detector and recorded by a computer. In this experiment, a computer control program, DCC, running on a PC to provide flexible control commands, was used. This program also provides analysis of data, such as peak finding and composition analysis for ternary epilayers. All motions of the diffractometer are controlled by stepping motors, through the computer and the Bede Minicam RS-232 interface system.

(a)

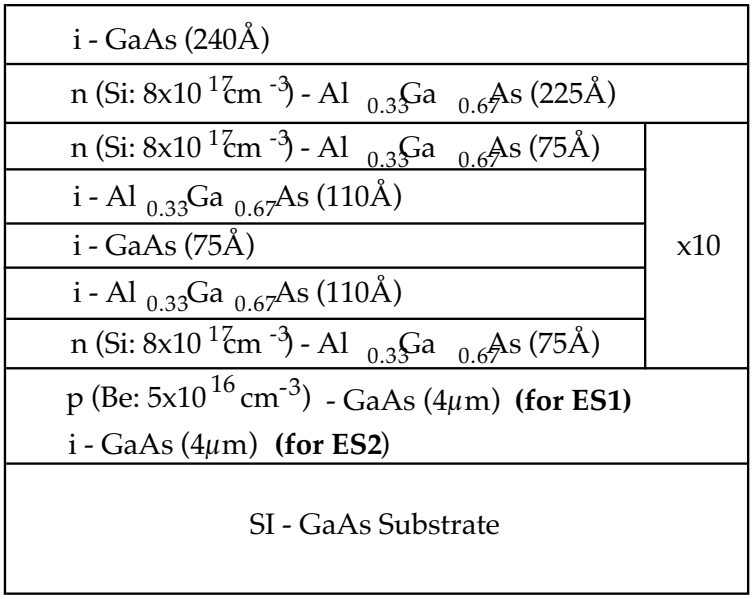

(b)

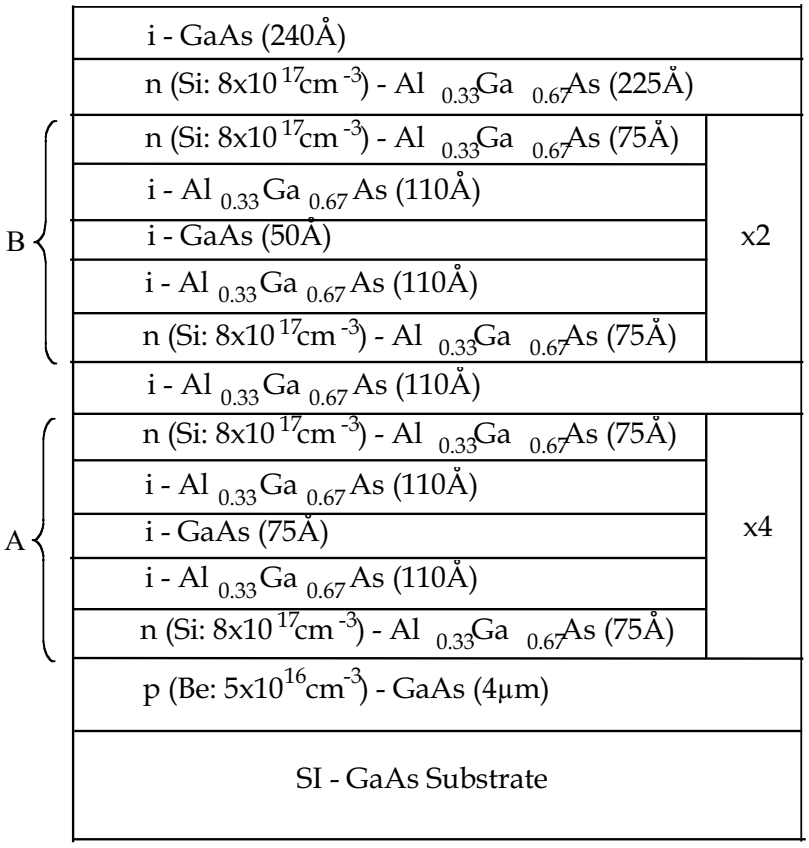

Figure 1. Schematic diagram of HELLISH-2 structure ; **(a)** For samples ES1 and ES2 and **(b)** For sample ES6.

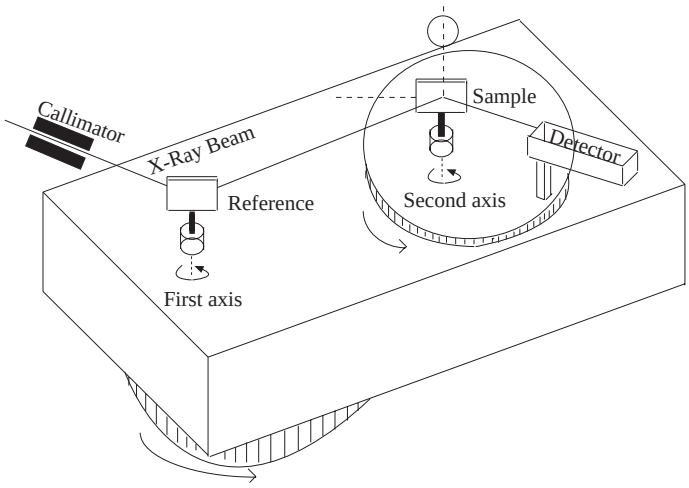

Figure 2. Schematic diagram of the experimental set-up in a nondispersive (+n, -m) setting in wavelength.

4. Analysis of Rocking Curves

The rocking curve of an MQW sample is quite complex. It may be analysed to give much of information required by crystal grower and device designer. In this work, the method of analysis developed by Segmuller et al. [7], Kervarac et al. [8] and Fewster [13, 14] were used. A typical example for an experimental rocking curve is shown in Figure 3 for sample ES2. In this figure the main peak is the substrate peak and the full width at half maximum of this peak provide a quantitative measure of the crystal perfection. The narrow rocking curve peaks permit the separation of closely matched layer and substrate reflections. Tilt should be optimised during the experiment to obtain narrow and higher intensity rocking curve; otherwise the position of the peaks may not be resolved, and information may be lost close to the peaks. Interference fringes may also vanish and therefore experimental rocking curves may not be compared directly with that obtained by computer simulation. Some epilayer defects, misorientation, mismatch, nonuniformity, and bending of epilayers with respect to the substrate that occur during growth affect the rocking curve. They result in the broadening and splitting of the peaks. The rocking curve is also broadened if the lattice spacing of the reference and specimen crystals is not equal. The broadening $d\theta$ is given by

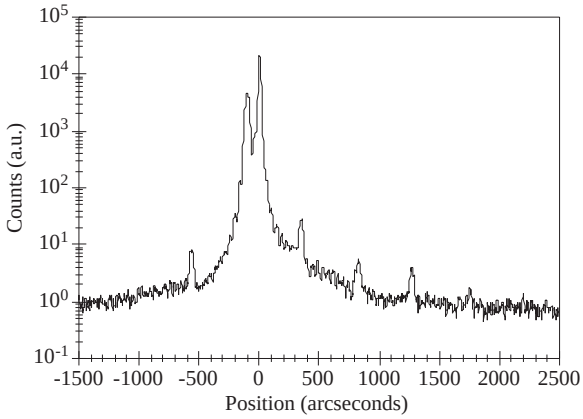

Figure 3. A typical example of experimental rocking curve for sample coded as ES2

$$d\theta = \frac{d\lambda}{\lambda}|\tan\theta_1 - \tan\theta_2|, \tag{4.1}$$

where θ_1 and θ_2 are the Bragg angles of the reference and specimen crystals, and $d\lambda$is the bandwidth of the x-ray wavelengths admitted by the collimator (this can be taken as the separation between the characteristic K_α lines).

The second highest peak on the left side of the substrate peak is known as the "zero-order" peak due to the Bragg reflection from the GaAs and $Al_xGa_{1-x}As$ components of the MQW. Figure 4 shows the expanded scale to reveal the zero order peak clearly. The peak separation between the substrate and zero-order reflection, due to having different lattice parameter in the epilayers with respect to the substrate, is related to the change of interplanar spacing normal to the substrate. If we call this separation δd, then the change in interplanar spacing is given through the equation

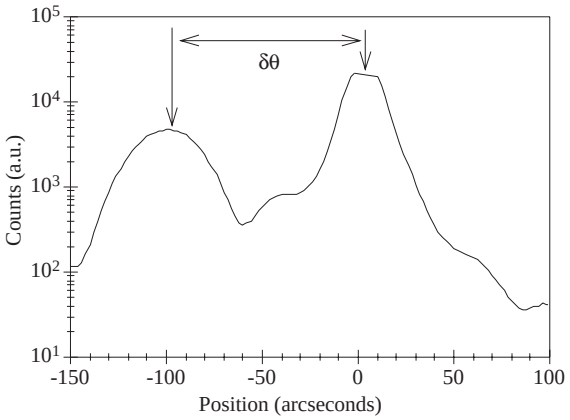

Figure 4. The expanded scale of Figure 3 to reveal the "zero order" peak.

$$\frac{\delta d}{d} = -\delta\theta \cot\theta_B \tag{4.2}$$

which is the differential form of the Bragg's Law. If the reflection is the usual symmetric 004, then the experimental mismatch is given by

$$m^* = \frac{\delta a}{a} = \frac{\delta d}{d} \tag{4.3}$$

Small-amplitude interference, or Pendellösung fringes, are seen on either side of the substrate peak. The expanded scale Pendellösung fringes are shown in Figure 5. The angular separation $\Delta\theta$ between two (more than two interference fringes can be used to get a more accurate value by averaging them) interference fringes maxima is related to the total epilayer thickness t as follows:

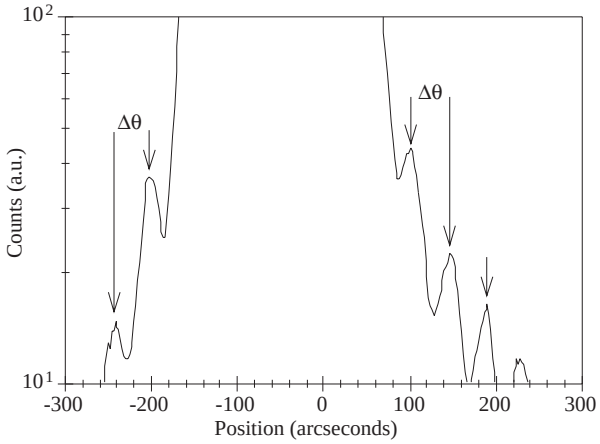

Figure 5. The expanded scale of Figure 3 to see the interference fringes for calculation of total epilayer thickness.

$$t = \frac{\lambda}{2\Delta\theta \cos\theta_B} \tag{4.4}$$

where λ is wavelength of the X-ray radiation and θ_B is the Bragg angle.

As is seen from Figure 3, there are sets of subsidiary "satellite peaks" on both sides of the "zero-order" peak. The closest peaks on both side of the zero-order peak are known as "first-order" peaks. The total thickness of the repeated MQW unit can be calculated by using the angular separation between the first-order peaks, which are arrayed symmetrically with respect to zero-order peak on both side of the rocking curve using the equation

$$p = \left(\frac{n_i - n_j}{2}\right) \frac{\lambda}{\sin\theta_i - \sin\theta_j} \tag{4.5}$$

where n_i and n_j show the satellite peak order and θ_i and θ_j are the diffraction angles. Higher order satellite peaks are distributed antismetrically in the rocking curve probably due to bending of epilayers with respect to the substrate during the growth.

By using the computer program using RADS (Rocking curve Analysis via Dynamical Simulation), which is based on the solution of Takagi-Taupin equations [15, 16], a generalised form of the dynamical theory of x-ray diffraction, was also performed for all three samples. Simulation of the rocking curve is an extremely powerful method for accurate interpretation of complex structures. A typical example for both experimental and simulated rocking curves is shown together for comparison for sample ES2 in Figure 6. The difference in the observed integrated intensity F_o and calculated structure factor F_c for all the observable satellites of the MQW unit is given as follows:

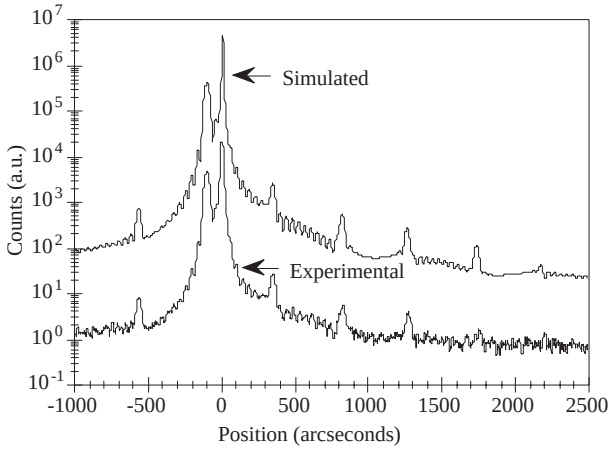

Figure 6. A typical example of experimental and simulated rocking curves for comparison for sample ES2.

$$R = \sum \frac{|F_o| - |F_c|}{|F_o|} \tag{4.6}$$

where R gives the correlation between the observed and simulated rocking curves. Smaller the values of R, the better. Having the quantum well width from photoluminescence measurements differences between the calculated and measured intensities can be minimised as a function of the well:barrier ratio.

5. Experimental Results

Double axis x-ray diffraction technique was performed for three samples ES1, ES2 and ES6. For sample ES1, the rocking curve was collected with a range of 10000 arcseconds centred on the [004] GaAs substrate with a stepsize of 2 arcseconds and the counting time of 10 seconds per step. It took about 14 hours to complete. Both experimental and simulated rocking curves are shown together for comparison in Figure 7. In this figure, the reflection that appeared at 14 arcsecond is the substrate peak with FWHM of 15.7 arcsecond and represents a good GaAs crystal. Lattice mismatch between epitaxial layers and the substrate is obtained at 388.1 ppm for this sample by using Equation (3). Total thickness of the epilayer is calculated as 4514 Å via Equation (4). The thickness of one period of the quantum well is found to be 403 Å from equation (5). From

photoluminescence measurement at 5 K the quantum well width is obtained as 71 Å. Therefore, well:barrier ratio is 71:332. Chemical composition cannot be directly calculated from the rocking curve for such complex structure. Simulation gives information about the composition. The Al concentration, x=0.33, taken from the growth menu was used for the simulation. Other parameters used during the simulation are given in Table 1. Excellent agreement between experimental and simulated rocking curves is obtained with these parameters as shown in Figure 7. The correlation factor is calculated as R=5.43% by using Equation (6) with well:barrier ratio as given above. As we studied in our previous work [12] input parameters of theoretical modelling from HELLISH-2 were directly taken from growth menu, however real device parameters from analysis of rocking curves were calculated approximately 10% less than that given by growth menu (see Figure 1). Since these parameters strongly affect output of the model (potential profiles and injected current density) they lead to us to reconsider the input parameters again in order to have an effective optimisation of HELLISH-2.

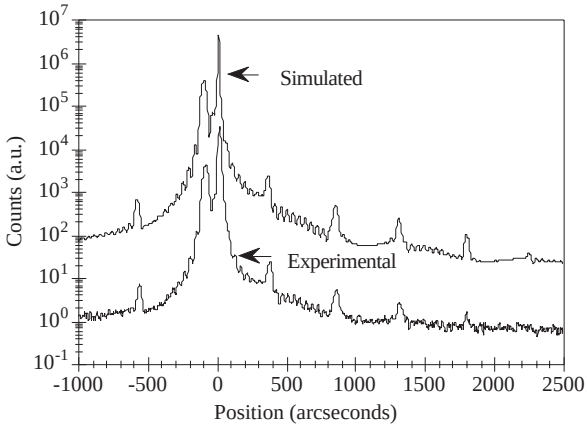

Figure 7. Experimental and simulated rocking curves for sample ES1.

Table 1. Simulation parameters used for all three samples.

Wavelength of x-ray radiation	$\lambda = 1.541$ Å
Polarisation	π (C=1) and σ (C=cos2θ) selected
Scan Range (arcsecond)	3500 arcsecons
Scan Step	2
Reference Crystal	Si
Bragg Angle	θ_B=14.23°
Reflection Indices	h k l : 1 1 1
Number of Reflection	1
Diffraction Geometry	Symmetric
Substrate Material	GaAs
Bragg Angle	θ_B=33.04°
Reflection Indices	h k l : 0 0 4
Reflection Orientation	Symmetric
Surface Normal Indices	h k l : 0 0 1

The rocking curves for ES2 and ES6 are shown in Figures 6 and 8, respectively. Excellent agreements are also obtained between experimental and simulation results for these samples. Since the structural parameters of ES2 are the same as ES1, except the doping density of the GaAs buffer layer which doesn't effect the experimental results so much, the rocking curve for ES2 is almost identical as that for ES1. However, ES6 has two periods of quantum wells with two different well widths, which are separated by 110 Å $Ga_xAl_{1-x}As$ barrier (Figure 5). The rocking curves are therefore very different from the previous samples, as shown in Figure 8. In this figure, higher order satellites peak and Pendellösung fringes vanish because of the destructive interference associated with these two different periods of MQW structures. Other parameters obtained from these two samples are given in Table 2.

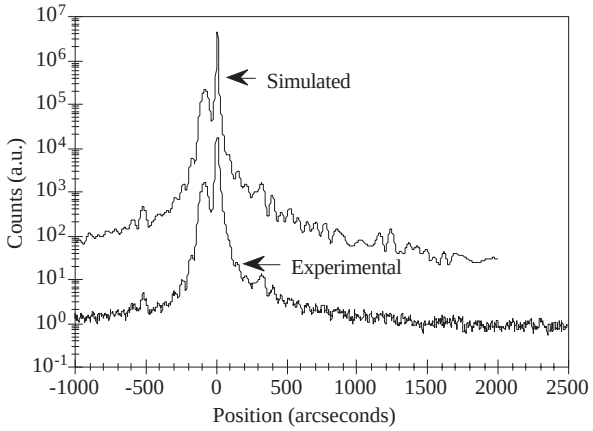

Figure 8. Experimental and simulated rocking curves for sample ES6.

Table 2. The parameters obtained from double axis x-ray diffraction rocking curves and simulation. [FWHM. Full width at half maximum, LM. Lattice mismatch, TET. Total epilayer thickness, TOPQW. Thickness of one period of quantum well]

	FWHM	LM	TET	TOPQW	Al-conts.	R
ES2	14.5arcsec	380.4ppm	4624Å	415Å	33%	6.80%
ES6	17.7arcsec	343.3ppm	3186Å	449Å	33%	6.34%

6. Conclusion

It has been shown that interference fringes and satellite peaks separation allow us to find the structural parameters of the MQW systems by using double axis x-ray diffraction and computer simulation. It has been realised that any small changes, such as quantum well width, barrier width and composition percentage, can strongly affect the experimental and simulated rocking curves. Doping does not affect the observed and simulated rocking curves. It has also been shown that two different period of repeated unit in the same structure vanishes the interference fringes and higher order satellites peaks due to destructive interference. Knowing the device parameters accurately, one can modify and optimise device parameters more effectively for higher efficient operation. Therefore, this characterisation technique, supported with a computer simulation, would be very useful for device designer in order to understand the device properties.

Acknowledgements

Author would like to thank Dr. N. Balkan, Physics Department of University of Essex, UK for his support and valuable discussion and would like to thank Prof. J. H. Wolter and his co-workers helping me to do this work in Eindhoven University of Technology, NL.

References

[1] X. Chu and B. K. Tanner, *Appl. Phys. Lett.,* **49**, (1986) 1773.

[2] B. M. Paine, *Mat. Res. Soc. Symp. Proc.* **Vol. 56,** (1986) 121.

[3] L. Tapfer, M. Ospelt and H. von Kanel, *J. Appl. Phys.* **67**, (1990) 1298.

[4] B. K. Tanner and M. A. G. Halliwell, *Semicond. Sci. Technol.,* **3**, (1988) 967.

[5] L. Francesio, P. Franzosi and G. Landgren, *J. Phys. D: Appl. Phys.,* **28**, (1995) A169.

[6] L. Tapfer and B. K. Ploog, *Phys. Rev.,* **B 40,** (1989) 9802.

[7] A. Segmuller, P. Krishna and L. Esaki, *J. Appl. Cryst.* **10,** (1977) 1.

[8] J. Kervarac, M. Baudet, J. Caulet, P. Auvary, Y. Y. Emeny and A. Regreny, *J. Appl. Cryst.* **17,** (1984) 196.

[9] N. Balkan, A. Teke, R. Gupta, A. Straw, J. H. Wolter and W. van der Vleuten, *Appl. Phys. Lett.* **67**, (1995) 935.

[10] R. Gupta, N. Balkan, A. Teke, A. Straw, and A. da Cunha, *Superlattices Microstructures,* **18**, (1995) 45.

[11] N. Balkan, A. da Cunha, A. O'Brien, A. Teke, R. Gupta, A. Straw, M. Ç. Arikan, in "Hot Carriers in Semiconductors", edited by K. Hess et al., Plenum Press, New York, (1996) 603.

[12] A. Teke, R. Gupta, N. Balkan, J. H. Wolter and W. van der Vleuten, Semicond. *Sci. Technol.,* **12**, (1997) 314.

[13] P. F. Fewster, *Philips J. Research,* **41**, (1986) 268.

[14] P. F. Fewster, *J. Appl. Cryst.,* **21**, (1988) 524.

[15] S. Takagi, *Acta Cryst.,* **2**, (1962) 241.

[16] D. Taupin, *Bull. Soc. Fr. Min. Cryst.,* **87**, (1964) 4960.